Journal of Molecular Liquids 387 (2023) 122606

Contents lists available at ScienceDirect

Journal of Molecular Liquids

journal homepage: www.elsevier.com/locate/molliq

Machine learning-assisted MD simulation of melting in superheated AlCu validates the Classical Nucleation Theory

Azat O. Tipeev [a,*], Roman E. Ryltsev [b,c], Nikolay M. Chtchelkatchev [d], Shiddhartha Ramprakash [e], Edgar D. Zanotto [a]

[a] Department of Materials Engineering, Federal University of São Carlos, 13565-905 São Carlos, SP, Brazil
[b] Institute of Metallurgy, Ural Branch of the Russian Academy of Sciences, 620016 Ekaterinburg, Russia
[c] Ural Federal University, 620002 Ekaterinburg, Russia
[d] Vereshchagin Institute for High Pressure Physics, Russian Academy of Sciences, 108840 Troitsk, Moscow, Russia
[e] National Institute of Technology Tiruchirappalli, 620015 Tamil Nadu, India

ARTICLE INFO

Keywords:
Superheating
Crystal melting
Nucleation
Binary alloy
Lindemann criterion
Critical nucleus
Molecular dynamics
Density functional theory
Machine learning

ABSTRACT

The validity of the Classical Nucleation Theory (CNT), the standard tool for describing and predicting nucleation kinetics in metastable systems, has been under scrutiny for almost a century. While the CNT is commonly employed to describe liquid → crystal and liquid ↔ vapor phase transitions, its application to the crystal → liquid case has been limited because of the experimental challenges in achieving superheating states and detecting homogeneous liquid nucleation. In this study, we performed comprehensive molecular dynamics (MD) simulations of spontaneous melting of a superheated AlCu crystal under atmospheric pressure at five temperatures, covering a superheating range of $T/T_L = 1.1$–1.3, where T_L is the liquidus temperature. Two realistic AlCu models were investigated: one described by the modified embedded atom method (MEAM) and the other by an interatomic potential generated by an artificial neural network machine learning (ML) approach, extensively trained on an *ab initio* dataset of liquid and crystal configurations. Fifty independent melting events were simulated at each temperature. By analyzing the distribution of melting times using the Poisson law, the homogeneous nucleation rate was determined through the mean lifetime method. Additionally, the Zeldovich factor, critical nucleus size, and work of formation were obtained using the mean first-passage time method, utilizing the disorder parameter based on atomic displacements (liquid-like atoms in the superheated crystal) as the reaction coordinate. Also, the effective atomic transport coefficient across the metastable crystal/critical liquid nucleus interface was determined by MD simulations as the interfacial attachment coefficient for nuclei growth rates. Using these simulation-generated data, the theoretical nucleation rates were calculated by the CNT with no fitting parameters. We found excellent agreement between the theoretically and MD-computed liquid nucleation rates for both MEAM and ML crystals. Notably, the effective solid-liquid interfacial free energy value obtained from the MD data aligns with its recent experimental measure. Moreover, the CNT qualitatively and quantitatively described the underlying details of liquid drop nucleation in our ML solid, unprecedentedly and accurately reproducing the kinetic prefactor and the size, formation energy, and growth rate of the critical nuclei. Thus, the melting of the AlCu model created through machine learning-processed quantum calculations, that is, not relying on hand-crafted interatomic potential functions, was successfully described by the CNT phenomenological formalism, without any adjustable parameters. This finding confirms the CNT as a very reliable descriptor of homogeneous nucleation in the superheated AlCu alloy and generalizes this theory as a powerful tool for analyzing and predicting the kinetics of crystal-liquid transitions.

1. Introduction

Crystalline solids usually start melting from the surface [1,2,3,4,5,6]. Indeed, because a solid surface is completely wetted by its own liquid, the creation of a liquid layer on a solid requires no work of formation of a new surface. As a result, it is very difficult to superheat a solid with an

* Corresponding author.
E-mail address: azattipeev@gmail.com (A.O. Tipeev).

https://doi.org/10.1016/j.molliq.2023.122606
Received 20 June 2023; Received in revised form 12 July 2023; Accepted 14 July 2023
Available online 17 July 2023

open surface; hence, crystals normally melt just above their equilibrium melting temperature. However, superheating can be achieved in certain special experimental conditions [7,8,9,10,11,12,13,14,15,16]. For example, surface melting can be suppressed if a solid is rapidly heated throughout its volume while maintaining a surface temperature lower than the melting temperature [7]. Superheating can also be achieved in laser-heated tiny crystalline clusters inserted into a medium with a higher melting temperature [16]. Finally, considerable superheatings can be achieved by ultrafast shock-wave compression of solids [14,15]. Employing shock-wave loading and intense laser irradiation, superheatings up to 43 % higher than the corresponding melting points were obtained for a number of elements and simple compounds [17].

Various theoretical approaches can be used to predict the maximum attainable superheating, based on thermodynamic, mechanical, and vibrational criteria [18,19]. The famous Lindemann melting criterion [20], based on the Einstein's theory of specific heat of crystals, states that melting occurs when the average atomic oscillation amplitude exceeds a certain threshold value; however, its universal applicability is still under debate [21,22,23]. Born proposed that the loss of stability in an unstressed crystal is linked to the vanishing of its shear modulus [24]. The achievable superheatings can also be described using a kinetic criterion based on the Classical Nucleation Theory (CNT) [25,26,27]. In this way, the maximum superheating corresponds to a certain (arbitrary defined) threshold nucleation rate [28,29].

The CNT [28,30,31] can also be utilized to describe the kinetics of homogeneous liquid nucleation in superheated isotropic crystals. According to this theory, the work of formation of a spherical critical nucleus, W_*, is given by.

$$W_* = \frac{16\pi\gamma^3}{3\rho_*^2(\Delta g + e)^2} \tag{1}$$

where γ is the solid–liquid interfacial free energy, ρ_* is the number density of the critical nucleus (i.e., the inverse of its molecular volume), e is the elastic strain energy, and Δg is the difference between the chemical potentials of liquid and crystal, i.e., the thermodynamic driving force for liquid nucleation defined by the difference between the nucleation and liquidus temperatures.

The work required for nucleation corresponds to a critical nucleus of radius.

$$R_* = \frac{-2\gamma}{\rho_*(\Delta g + e)} \tag{2}$$

It should be noted that e takes positive values, whereas Δg is negative in the metastable region. For a phase transition to occur, the condition $\Delta g + e < 0$ must be met, meaning that the energy gained from the formation of a thermodynamically more stable phase must exceed the energy cost of establishing a field of internal stresses. However, just beyond the melting line, at small superheatings, $\Delta g + e > 0$ can be established, resulting in the absence of homogeneous nucleation [32].

The stationary nucleation rate, J, i.e., the average number of viable nuclei formed per unit time and volume, is given by [33].

$$J = \rho \mathscr{D}_* Z_* \exp\left(-\frac{W_*}{k_B T}\right) \tag{3}$$

where ρ is the crystal number density, k_B is the Boltzmann constant, $\mathscr{D}_*$ is the effective atomic transport coefficient across the metastable phase/critical nucleus interface, and Z_* is the dimensionless Zeldovich factor, which characterizes the curvature of the nucleation barrier in the vicinity of critical size,

$$Z_* = \left(\frac{W_*/k_B T}{3\pi n_*^2}\right)^{1/2} = \left(\frac{4R_*^2\gamma}{9k_B T n_*^2}\right)^{1/2} = \left(\frac{|\Delta g + e|}{6\pi n_* k_B T}\right)^{1/2} \tag{4}$$

where n_* is the number of atoms in the critical nucleus.

The Turnbull-Fisher expression, initially derived for liquid crystallization from the absolute reaction rate theory [34], may be adopted [30,35] to evaluate the transport coefficient for crystal melting:

$$\mathscr{D}_* = i_* \frac{kT}{h} \exp\left(-\frac{E_*}{kT}\right) \tag{5}$$

where i_* is the number of atoms on the surface of the critical nucleus, h is the Planck constant, and E_* is the activation energy for the transition of atoms from the metastable substance to the new-phase nuclei. However, E_* is normally unknown and usually estimated as the activation energy for atomic diffusion in the medium. This activation energy will be determined later in this study.

Experimental measurement of all variables in Eqs. 1–5 is extremely difficult or even impossible, since nucleation typically occurs at the nanometer scale and on timescales of pico- to nano-seconds. Notable advances have been made in experiments involving colloidal systems [36,37,38]. Their ~ 1 μm diameter particles were tracked individually by different microscopy techniques, allowing the direct observation of crystal lattice destruction during melting. However, some nucleation parameters, such as interfacial free energy and critical cluster size, cannot be directly observed. As a result, a comprehensive examination of theoretical nucleation models is very challenging [4,17,30,35,39].

In the past few decades, computer simulations have become a potent tool in phase transition research [40]. Specifically, molecular dynamics (MD) simulations enable the study of homogeneous melting at an atomistic level and on a timescale < 1 μs, thus yielding thought-provoking insights into the melting mechanisms of various crystals: Lennard-Jones (LJ) [41,42,43], Al [44,45,46,47], Al-based alloys [47], Cu [48,49], Fe [50], Ta [21,22,49], Pb [51], CoCrFeNiMn [23], methane hydrates [52], benzene [53], and ice *Ih* [54,55,56]. Through advanced computational methods, MD simulations provide uniquely valuable information about the properties of nanosized nuclei, thus serving as a powerful tool to test nucleation theories [25,57,58,48,42,43,59]. However, to the best of our knowledge, only three studies [42,43,59] have conducted a detailed comparison between the theoretically calculated nucleation parameters and those obtained through MD simulations using a LJ toy model. **The lack of similar analysis for multicomponent crystalline compounds described by realistic interatomic potentials is the primary motivation for this study.** Therefore, we focused on a theoretical and computational study of the melting phenomenon in an Aluminum-Copper alloy – a material of enormous technological significance in the aerospace and automobile industries [60,61,62], among others. Superheated AlCu is commonly utilized in the processing of high-temperature materials, namely, laser- and electron-beam welding to create robust and high-quality joints between diverse metal parts [63]. However, experimental studies on AlCu melting are relatively scarce [64,65,66,67,68] because of the challenges associated with achieving superheats, as previously mentioned.

The theoretical analysis of nucleation also becomes more intricate when dealing with multicomponent systems [31,69,70]. In the case of multicomponent nucleation, a cluster is formed with a specific composition that is dictated by the equilibrium conditions. Subsequently, the thermodynamic driving force Δg and the interfacial free energy γ are determined for this particular composition of the newly evolving phase. This study utilizes effective values of Δg and γ, as outlined in Ref. [31].

Turning to MD simulations, it is important to note that they crucially rely on the interatomic potential employed. Moreover, proper investigation of solid–liquid phase transformation using MD calculations can be problematic because of the structure-dependent parameterization of conventional potentials [71]. Fortunately, in this regard, machine learning (ML) approaches offer a revolutionary solution. Over the past decade, ML algorithms have become an important tool in calculus-based materials science and condensed matter physics because of their impressive ability to accelerate the discovery of materials and explain their behavior, among other applications [72,73,74,75,76,77,78,79]. Data-driven ML approaches have also been effectively used to construct complex interatomic potentials with first-principles accuracy at a

reasonable computational cost [80,81,82,83,84]. When applied to phase transition studies, these sophisticated ML models can provide valuable insights into experimental observations. For example, the experimental extreme supercooling of gallium was elucidated by an exceedingly large activation barrier for nucleation, uncovered through a crystallization study using a ML model [85].

Considering the aforementioned arguments, the two main objectives of this comprehensive study are: (i) to obtain crucial properties that describe liquid nucleation in superheated AlCu crystals, realistically simulated using both a traditional and a ML model, in a wide range of superheatings, and (ii) to test the validity of the CNT in predicting liquid nucleation rates in this important material. To accomplish this task, we developed a reliable AlCu force field using a neural network machine learning algorithm that was extensively trained on massive *ab initio* data of both AlCu crystal and liquid configurations.

This paper is structured as follows: Section 2 presents the mean lifetime and the mean first-passage time methods, as well as the MD models under investigation; the computational and theoretical results and discussion on AlCu crystal melting are given in Section 3; our conclusions are summarized in Section 4.

2. MD models and computational methods used

2.1. The MEAM and ML models

We studied the homogeneous melting of AlCu crystals under isothermal-isobaric conditions at atmospheric pressure using two computational models. The interatomic interaction in the first model was described by the second nearest-neighbor modified embedded atom method, as reported in Ref. [86]. This potential was derived from the original semi-empirical MEAM [87,88] by extending the interaction range to include the second nearest-neighbors [89,90], which improved the model stability and enabled better prediction of crystal-liquid coexistence properties – an important factor for the first-order phase transition studied.

We also implemented a neural network machine learning-based interatomic potential for a second model utilizing two strategies. The first involved training the potential only on liquid configurations without any prior knowledge of possible crystal structures, whereas the second involved training on both liquid and crystal configurations. These two ML potentials are referred to as ML-*l* and ML-*sl*, respectively. The development of these two ML potentials enables the study of the liquid–solid structural inheritance [91], contributing to a deeper understanding of this cutting-edge class of interatomic potentials.

We developed the AlCu ML interatomic potentials using the free and open-source DeePMD software [83], which employs feedforward deep neural networks to approximate the potential energy surface of many-particle systems. The training *ab initio* datasets were generated by an active learning strategy realized in the DP-GEN package [83]. The *ab initio* calculations were based on the Density Functional Theory (DFT) as implemented in the VASP code [92]. In the first stage, a few hundred *ab initio* trajectories were used to train an ensemble of four ML potentials, each with different initializations of neural network weights. Subsequently, we conducted MD simulations with these ML models under varying temperatures, pressures, and concentrations. The MD configurations that showed a maximum deviation, δ, ranging from 5 to 15 % between the forces predicted by the ML models and those obtained through the DFT calculations were added to the training dataset. Afterwards, we retrained the ML models on the extended dataset and ran new MD simulations while enforcing the δ criterion to control their accuracy. This active learning process was carried out iteratively until the criterion $\delta < 5$ % was met for all MD configurations, resulting in the development of the ML potential with uniform accuracy under specific thermodynamic conditions. In this way, we performed ML-assisted MD simulations at temperatures ranging from 800 to 2000 K and at three isobars: −10, 0.0, and 10 kbar. The Al, $Al_{75}Cu_{25}$, $Al_{50}Cu_{50}$, $Al_{25}Cu_{75}$, and Cu liquid configurations were considered in the ML-*l* potential development. In the ML-*sl* potential creation, we also included the following crystalline configurations: Al (fcc), Al_2Cu (θ-phase, I4/mcm), $Al_{50}Cu_{50}$ (C12/m1), $AlCu_3$ (β-phase, Pm3m), and Cu (fcc). The training dataset comprised approximately 10,000 DFT configurations, each containing 512 atoms. More technical details on both the *ab initio* calculations and the ML procedure can be found in Ref. [93]. In Ref. [94], the ML potentials developed underwent comprehensive and thorough validation using experimental and *ab initio* data pertaining to structural, thermodynamic, and transport properties, as well as evaluating their computational performance. Overall, the resulting ML potentials provided nearly *ab initio* accuracy and allowed us to achieve a computational cost at least three orders of magnitude (o.m.) smaller than that using DFT simulations.

The AlCu crystals under the melting study were composed of $N = 11664$ atoms arranged in a cubic cell with periodic boundary conditions in three dimensions. The structure of the AlCu crystals was B2, characterized by the replacement of a Cu atom with an Al atom at the body-centered position. This structure was selected because of its most negative formation energy, as determined by the MEAM model at the liquidus temperature, $T_L = 1170$ K[86], that is, the most thermodynamically stable lattice.

The accurate prediction of the equilibrium temperature in ML models is a challenging task [75,77,95,96,97]. We determined the liquidus temperature of our AlCu ML models at atmospheric pressure using the crystal-liquid equilibrium coexistence method [98,99]. The corresponding two-phase MD simulations were performed with the B2-structured crystal oriented in the (1 0 0) direction relative to the liquid. By monitoring the alteration in the total potential energy and visualizing the atomic configurations over 2 ns simulations in the *NpT* ensemble, we discovered that the two-phase ML-*l* (ML-*sl*) system always crystallized at temperatures $T \leqslant 880$ K (820 K) and melted at $T \geqslant 890$ K (830 K). Thus, the liquidus temperatures for the ML-*l* and ML-*sl* models were estimated as $T_L = 885(4)$ K and $T_L = 825(4)$ K, respectively. Hereafter, the number in parenthesis indicates the uncertainty in the last significant digit. These values of T_L are lower than the experimental one, $T \approx 1100$ K, and fall within the temperature range of AlCu solid–solid transitions [100]. One can thus hypothesize that the decay of the ML crystals may be the first stage of their transformation into a more stable crystalline state through the formation of a supercooled liquid as an intermediate phase. Such a phenomenon was recently observed in experiments conducted on a rapidly heated $Au_{70}Cu_{5.5}Ag_{7.5}Si_{17}$ metallic system [101]. However, investigating this intriguing hypothesis is beyond the scope of this paper and requires further research.

Having established the liquidus temperatures of the current models, a perfect B2-structured AlCu crystal sample was created at $T = T_L$ under 1 bar. Next, after 10 ns of equilibration in *NpT* conditions, 50 stable configurations were collected for 5 ns for each studied model. The superheated (stretched) crystals were obtained by isobaric heating at a rate of $\Delta T/\Delta t = 10^{12}$ K/s.

The MD simulations were performed by parallel calculations in the free and open-source LAMMPS software [102,103]. Following Ref. [44], the timestep in the simulations was set at 2 fs, which is shorter than the typical atomic vibrational period in solids. The relaxation times for the thermostat and the barostat were set to 0.2 and 2 ps, respectively.

2.2. The mean lifetime (MLT) method

The spontaneous formation of a liquid nucleus in a superheated crystal is a stochastic event described by the Poisson probability distribution [104]:

$$P(m,\tau) = (m!)^{-1}(\lambda\tau)^m \exp(-\lambda\tau) \tag{6}$$

where $P(m,\tau)$ is the probability of forming m supercritical nuclei by time τ, λ is the formation rate of supercritical nuclei, $\lambda = JV$, and V is the

box volume.

In the high metastability region (large superheating), the formation of one viable nucleus is sufficient to initiate a phase transition. Taking $m = 1$ in Eq. (6), yields the probability of formation of one supercritical nucleus by time τ:

$$P(1,\tau) = \lambda\tau\exp(-\lambda\tau) \tag{7}$$

Consider $\mathcal{N}$ independent nucleation experiments. The number of nucleation events from τ to $\tau + \Delta\tau$, according to Eq. (7), is equal to

$$k = \mathcal{N}\lambda\Delta\tau\exp(-\lambda\tau) \tag{8}$$

Thus, analyzing the distribution of nucleation times from Eq. (8), one can obtain λ and, consequently, the nucleation rate, $J = \lambda V$[28,105].

The average time of the first critical nucleus expectation or the mean lifetime of a metastable sample is given by:

$$\overline{\tau} = \int_0^\infty \lambda\tau\exp(-\lambda\tau)d\tau = \lambda^{-1} = (JV)^{-1} \tag{9}$$

Accurately measuring the appearance time of a supercritical liquid nucleus in real crystal melting experiments is very challenging, and is only possible in certain cases, such as in colloids [38]. Therefore, liquid nucleation events are usually recorded indirectly by a secondary feature, such as a change in the diffraction pattern or in electrical resistance due to the formation of a large amount of a new phase, as well as by various calorimetric or radiation techniques. As a result, these nucleation times include the expectation time for the first critical nucleus and the time for its growth to registrable size. The times associated with the growth of the nucleus and the establishment of a stationary process can be easily detected by Eq. (8), since the probability of a single event in the Poisson process is independent of the origin time.

The MLT method was first used in experimental studies of spontaneous boiling up of superheated liquids [28]. In computer simulations, this method has been successfully employed in studying cavitation in tensile-stressed liquids [106,107], spontaneous crystallization of supercooled liquids [105,108], and melting of a superheated crystals [42,45,48,57,59].

2.3. The mean first-passage time (MFPT) method

Nucleation is a thermally activated process. In computer simulations, the kinetics of these processes can be analyzed using the mean first-passage time method [109,110]. "First-passage time" refers to the time taken by a state variable to reach a certain value. In nucleation simulations, the state variable or a reaction coordinate is usually the size of the largest nucleus of the new phase, $n_{\max}$ [110]. The mean time for the appearance of a nucleus of any given size, $\langle\tau(n)\rangle$, can be obtained from a set of $n_{\max}(\tau)$. According to the MFPT formalism, the $\langle\tau(n)\rangle$ dependence is given by:

$$\langle\tau(n)\rangle = \frac{\overline{\tau}}{2}\left\{1 + \mathrm{erf}\left[Z_*\sqrt{\pi}\,(n - n_*)\right]\right\} \tag{10}$$

where $\mathrm{erf}(x)$ is the error function and n_* is the number of atoms in the critical nucleus.

Thus, by fitting the $\langle\tau(n)\rangle$ data with Eq. (10), three important nucleation parameters can be obtained: n_*, Z_*, and $\overline{\tau}$. Moreover, the MFPT method also enables determination of the work of formation for the critical nucleus, W_* [111]. Noteworthy, careful consideration should be given to the choice of the reaction coordinate and time resolution [112], as they greatly affect the accuracy of the MFPT results. The MFPT approach has been effectively applied in nucleation computational studies in condensation [110,113], crystallization [105,114,115], and melting [59].

3. Results and discussion

3.1. Melting of superheated AlCu crystals in MD models

Fig. 1 shows the temperature dependence of the crystal d_S and liquid d_L densities of AlCu in a specified region of interest. The experimental values were obtained by an accurate method of penetrating gamma radiation [116], based on the Beer-Lambert-Bouguer law of light beam attenuation by an absorbing substance. The MD data of $d_S(T)$ were obtained by heating a homogeneous crystal sample from room temperature up to complete melting, with a heating rate of $\Delta T/\Delta t = 5{\cdot}10^{11}$ K/s. The melted sample was then cooled at the same rate to calculate $d_L(T)$. We found a good agreement between the experimental and computational density values, with differences of only ~ 15 % (~6 %) between the MEAM (ML) models and the experimental values.

Since the liquidus temperatures were different for each MD model, we implemented a unified temperature scale, T/T_L. In this way, the melting process was studied in a range of superheatings: $T/T_L = 1.11 - 1.30$. Such superheatings can be achieved in modern experiments [17]; however, it is challenging to investigate experimentally the crystal decay at a microscopic level. On the other hand, computer simulations allow us to track the melting phenomenon at an atomic scale, providing insight into the underlying mechanisms of this process.

Fig. 2 displays the typical time dependence of the density of a superheated AlCu crystal. A decrease in density due to crystal decay is observed, resulting from the nucleation and substantial growth of a liquid drop. The melting time was taken as the time when the total system density decreased by 1 % of its initial value. This time was the sum of three contributions: (i) expectation time for the first viable nucleus; (ii) growth time; (iii) time-lag associated with establishing both a stationary flow of nuclei [33] and the thermodynamic parameters after a transient process to the temperature under investigation.

Fig. 3 shows the distributions of the melting times at $T/T_L = 1.1$ and 1.3, which are well fitted with a Poisson distribution, Eq. (8). Extracting

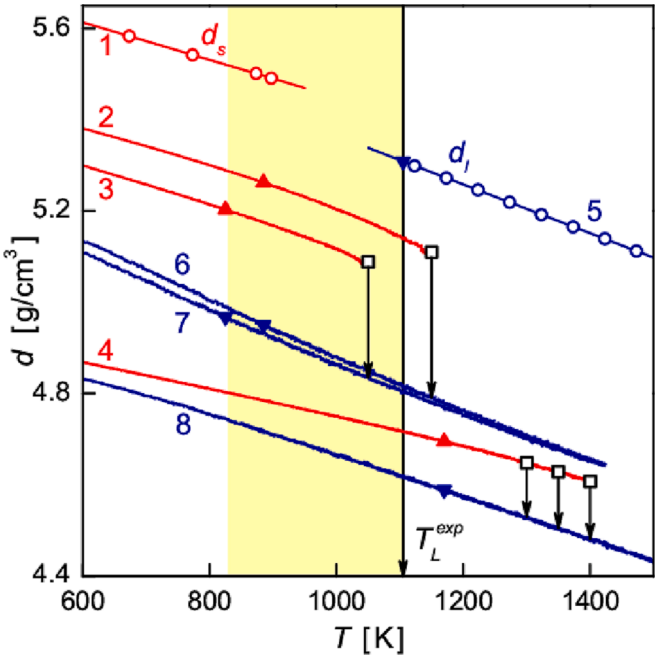

Fig. 1. Temperature dependence of the crystal d_s and liquid d_l density of AlCu along 1 bar isobar: experimental data on d_s(1) and d_l (5) from Ref. [116]; current MD calculation of ML-*l* system, d_s(2) and d_l (6); ML-*sl*, d_s(3) and d_l (7); MEAM, d_s(4) and d_l (8). The corresponding liquidus temperatures, T_L, are indicated by triangles. The experimental value of T_L is shown by a vertical line. The five superheating states under study are specified by squares. The temperature range of the AlCu solid-solid transitions [100] is shown in yellow.

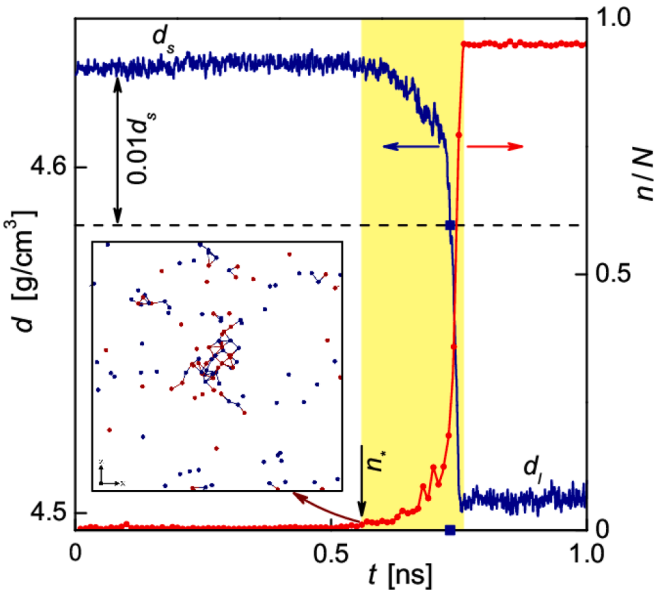

Fig. 2. Time dependence of the density of a melting AlCu MEAM crystal and the number of liquid-like atoms, normalized by the total number of atoms, $T = 1.15 \cdot T_L$. The horizontal line shows a 1 % density drop, which determines the melting time in the MLT method. The time interval of the melting process, 0.1 ns, is shown in yellow. **Inset:** 2D projection of the system configuration at the melting onset; only liquid-like atoms are shown.

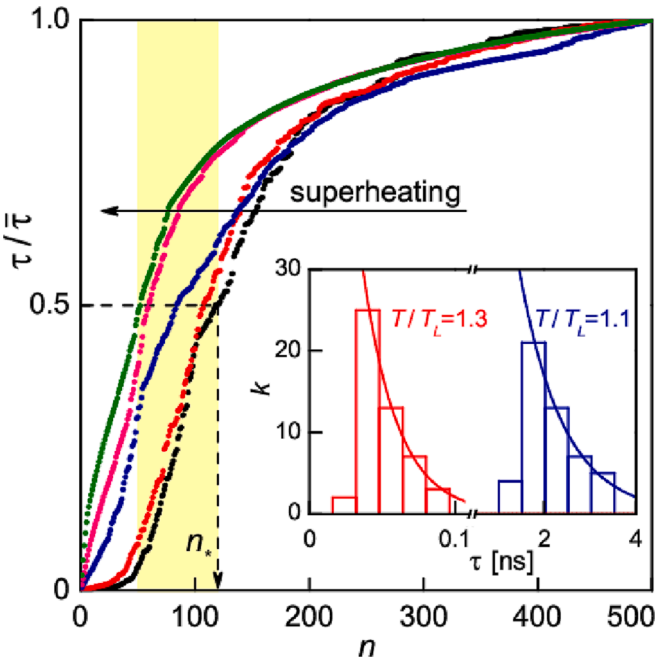

Fig. 3. Mean first-passage times *vs.* liquid nucleus size for five superheatings: $T/T_L = 1.11$, 1.15, 1.20, 1.27 and 1.30. The horizontal arrow denotes the direction of superheat increase. The critical nucleus size corresponds to $\tau/\bar{\tau} = 0.5$, Eq. (10), and is highlighted in yellow. The atomic transport coefficient, $\mathscr{D}_*$, was calculated within the range of $\tau/\bar{\tau} = 0.4 - 0.6$. **Inset:** Histograms of the AlCu melting time distribution for the lowest and highest superheatings studied. The smooth curves are the Poisson distribution, Eq. (8).

both the nucleus growth times and nucleation time-lags was possible because of the independence of the probability of an individual event onset from the beginning of the time reading [105]. The mean lifetime, $\bar{\tau} = 1/\lambda$, was obtained as a fitting parameter, with an uncertainty of $\sigma_{\bar{\tau}} = \bar{\tau} \cdot \mathscr{N}^{-0.5} \approx 0.14 \cdot \bar{\tau}$ [28]. In the superheating range studied, the mean nucleation times changed by 2 o.m., $\bar{\tau} = 3 \cdot 10^{-11} - 2 \cdot 10^{-9}$ s.

Using the MD values of $\bar{\tau}$ and V, the nucleation rate, J, was calculated by the MLT method from Eq. (9). In this way, J increases from $J = 2.6(4) \cdot 10^{33}$ s^{-1}m^{-3} at $T/T_L = 1.11$ to $J = 2.0(3) \cdot 10^{35}$ s^{-1}m^{-3} at $T/T_L = 1.30$. These high nucleation rates observed are typical in brute-force MD simulations [40,99] and, notably, exceed those obtained experimentally at ~ 3 %-superheated Al–3.7wt.%Cu melting using scanning electron microscopy: 10^{13} to 10^{15} s^{-1} m^{-3} [67]. To simulate homogeneous melting in thermodynamic states with lower experimental nucleation rates (higher nucleation times), a significant improvement in computational resources is necessary, especially for systems described by complex ML potentials. Most likely, similarly to the crystallization computational studies at moderate supercooling, advanced sophisticated methods can be employed to accelerate the formation of liquid nuclei in crystals [40]. Entering a higher superheating region, the melting times become extremely short, $\bar{\tau} < 1$ ps or dozens of MD time-steps, resulting in melting the crystal as early as during the heating path to the target temperature.

Another route to calculate the nucleation time is by tracking the size of evolving new-phase fragments and analyzing them by the MFPT formalism [110]. To employ this approach, a suitable reaction coordinate should be defined in a univocal manner. In crystallization studies, the order parameter, referred to the number of crystal-like atoms in a supercooled liquid, is often used as the reaction coordinate. In this study, we utilized a disorder parameter, which was determined via the amount of liquid-like atoms in the superheated crystal, i.e., atoms that belong to the liquid phase. To identify them, the atomic coordinates were stored every 10 picoseconds and the atomic displacements were analyzed [51]. The locations of large displacements during melting were different in the ML and MEAM crystals. In the ML case, we observed large atomic jumps only in a certain region, whereas in the MEAM case, larger jumps were localized not only in some regions, but also randomly throughout the volume. This behavior is attributed to the decrease in the diffusion activation barrier with temperature. However, further research is required to investigate the possible alterations in the melting mechanism [21,23].

The atoms that moved further than a threshold value for 10 ps were considered to be liquid-like or mobile [8,41,50]. The temperature-dependent threshold was selected to identify ≈ 95 % of the atoms in a system as mobile in the molten state at a given temperature. It varied from 1.5 to 1.9Å. Fast single atoms without mobile neighbors were excluded from the analysis. A group of n mobile atoms, located within a distance less than a lattice constant from each other, was considered as a liquid nucleus of size n (Inset in Fig. 2). In this way, we found that each melting event was always initiated by a single critical nucleus. Both the MEAM and ML models showed that the number of mobile atoms perfectly correlated with the increase in system enthalpy and the decrease in density resulting from solid decay (Fig. 2). Thus, this result supports the Lindemann criterion for melting onset, that is, a crystal starts to melt when the atomic oscillations in the lattice reach a critical value [20]. Furthermore, liquid formation always occurred in regions of the mobile atoms (precursors to melting); therefore, liquid nucleation can be considered a two step process: superheated crystal – domain of mobile atoms – liquid nucleus. This finding agrees with experimental evidence of melting of a colloidal crystal composed of *N*-isopropylacrylamide microgel spheres, where a liquid drop nucleated in a zone of fast-moving particles [36].

After developing the procedure for determining the liquid nucleus size, 50 $n(t)$ dependencies were collected during crystal melting at each temperature. The time of first appearance of a liquid cluster of a certain size, $\tau(n)$, was determined for every computational experiment. The averaged $\langle\tau(n)\rangle$ curve demonstrates a typical S-shape at moderate superheatings (Fig. 3), as predicted by the MFPT approach [110]. However, at high superheatings, a deviation from the theoretical shape

was observed, which was earlier reported in a MFPT study on crystal nucleation of a deeply supercooled LJ liquid [115]. The MFPT nucleation times, $\bar{\tau}$, and, consequently, the nucleation rates are agree well with those determined by the MLT method (Table 1). The coincidence of $\bar{\tau}$ and J, determined by the MLT and MFPT methods, was established earlier in crystal nucleation analysis [105]. Along with $\bar{\tau}$, the critical size, n_*, and the Zeldovich factor, Z_*, were obtained by fitting the $\langle\tau(n)\rangle$ dependence with Eq. (10). Both $n_* = 50-120$ and $Z_* = 0.01-0.02$ showed adequate values (Fig. 4). The higher the superheating, the smaller the critical nucleus size found, which agrees with the CNT. Assuming that the number density of the liquid nuclei, ρ_*, is equal to that of the bulk liquid at a given temperature, the radii of the critical nuclei were determined as $R_* = (3n_*/4\pi\rho_*)^{1/3}$, and were $R_* = (0.7-0.8)$ nm.

3.2. Comparison of theoretically and directly determined nucleation rates

First, using the critical size, n_*, and the Zeldovich factor, Z_*, obtained by the MFPT method, the work of nucleus formation was calculated from Eq. (4) as $W_* = 3\pi n_*^2 Z_*^2 k_B T$. In this way, the height of the activation barrier, W_*/k_BT, ranges from 10 to 12. These values are comparable to those found in typical brute-force nucleation MD studies in superheated and supercooled liquids, and in supersaturated vapor, where W_*/k_BT normally does not exceed 20–25 [107,117,118]. Our nucleation barrier values align with the CNT analysis of experimental melting, where $W_*/k_BT = 30$ has been found [30,35].

The work, W_*, was calculated using the simulation data by Eq. (4), instead of Eq. (1), to avoid the unknown values of the interfacial free energy, γ. The use of approximations for $\gamma(T)$ may lead to significant overestimations of W_*. For example, the interfacial free energy was considered to be equal to that at a flat crystal/liquid interface, $\gamma(T) = \gamma_\infty$, for homogeneous melting of a LJ crystal [59], which leads to a huge theoretical nucleation barrier, $W_*/k_BT \approx 50-200$. As a result, the CNT nucleation rates were 16–70 o.m. lower than those directly calculated by MD. However, these high activation barriers obtained cannot be overcome in brute-force MD simulations, even for a fast-computed LJ model, where the barrier $W_* = 50{\cdot}k_BT$ corresponds to a nucleation rate $J \approx 10^{18}$ s^{-1}m^{-3} [119]. To reach this rate by direct simulation, even in a one-billion-atom system, the average waiting time for the first viable nucleus would be ~ 10 s, while typical MD times do not exceed 1 μs.

The driving force was calculated from Eq. (4) as $|\Delta g + e| = 6\pi n_* Z_*^2 k_B T$. The interfacial free energy, γ, was then determined from Eq. (2) as $\gamma = |\Delta g + e|\rho_* R_*/2$. As anticipated, the value of $|\Delta g + e|/k_BT$ increases with superheating, rising from 0.20 at $T/T_L = 1.11$ to 0.39 at $T/T_L = 1.30$. In contrast, γ remains nearly constant, with a value of 0.10(1) J/m^2, agreeing well with the experimental estimations available, $\gamma = 0.12(2)$ J/m^2 [68] and 0.09–0.16 J/m^2 [120].

Finally, the effective atomic transport coefficient, $\mathscr{D}_*$, was obtained as the attachment coefficient for nuclei growth rates from the MFPT curves, $\mathscr{D}_* = dn(t)/dt$, in the vicinity of the critical size, $n = n_*$. In this way, $\mathscr{D}_*$ takes values in the range from 10^{11} to $3{\cdot}10^{12}$ s^{-1}, and follows the Arrhenius law, as shown in Fig. 4.

Table 1
Melting parameters of AlCu crystals for $p = 1$ bar at five superheatings, T/T_L.

Quantity	Superheating, T/T_L				
	1.11	1.15	1.20	1.27	1.30
Model	MEAM	MEAM	MEAM	ML-*sl*	ML-*l*
T, K	1300	1350	1400	1050	1150
d_s, g/cm^3	4.65	4.63	4.61	5.09	5.11
d_l, g/cm^3	4.53	4.50	4.48	4.83	4.79
$\bar{\tau}$, s, MLT	$2.1{\cdot}10^{-9}$	$6.6{\cdot}10^{-10}$	$1.7{\cdot}10^{-10}$	$6.8{\cdot}10^{-11}$	$2.9{\cdot}10^{-11}$
$\bar{\tau}$, s, MFPT	$1.7{\cdot}10^{-9}$	$6.0{\cdot}10^{-10}$	$1.4{\cdot}10^{-10}$	$9.4{\cdot}10^{-11}$	$6.1{\cdot}10^{-11}$
J, s^{-1}m^{-3}, MLT	$2.6{\cdot}10^{33}$	$7.9{\cdot}10^{33}$	$3.2{\cdot}10^{34}$	$8.5{\cdot}10^{34}$	$2.0{\cdot}10^{35}$
J, s^{-1}m^{-3}, MFPT	$3.1{\cdot}10^{33}$	$8.8{\cdot}10^{33}$	$3.7{\cdot}10^{34}$	$6.2{\cdot}10^{34}$	$9.6{\cdot}10^{34}$
J, s^{-1}m^{-3}, CNT, Eq. (11)	$4.2{\cdot}10^{32}$	$2.6{\cdot}10^{33}$	$1.0{\cdot}10^{34}$	$7.5{\cdot}10^{34}$	$1.6{\cdot}10^{35}$

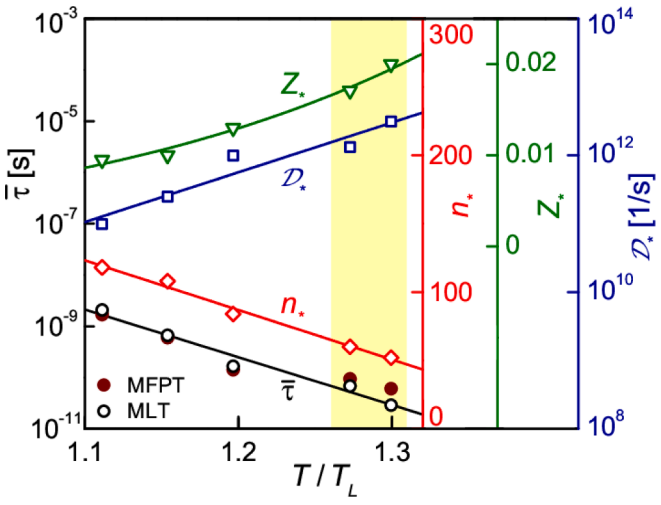

Fig. 4. Mean nucleation time, $\bar{\tau}$, determined by the MLT and MFPT methods, atomic transport coefficient, $\mathscr{D}_*$, number of atoms in the critical nucleus, n_*, and Zeldovich factor, Z_*, *vs.* superheating, T/T_L. The region studied by ML crystals is highlighted in yellow.

Using the MD values of the transport coefficient, $\mathscr{D}_*(T)$, and the number of atoms in the critical nucleus, $n_*(T)$, the activation energy, E_*, was estimated from Eq. (5). Because of the small nuclei size, whose radii do not exceed 1 nm, the number of surface atoms in Eq. (5) is assumed to be equal to half the total number of atoms in the critical nucleus at any given temperature, i.e., $i_*(T) = n_*(T)/2$ [119,121]. In this way, E_* decreases with temperature, as expected, ranging from 5 to 10 k_BT. Consequently, the kinetic barrier was found to be lower than the

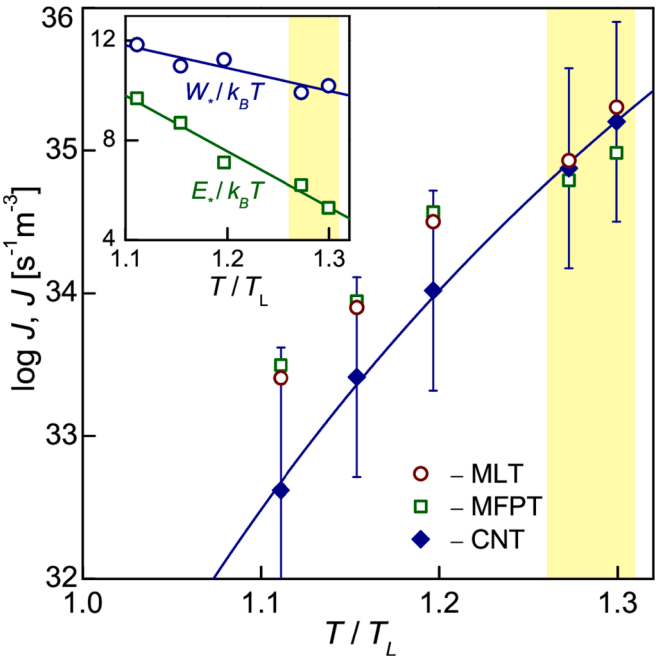

Fig. 5. Temperature dependence of the nucleation rate, J at $p = 1$ bar. The methods used are specified in the legend. The size of the symbols in MLT and MFPT J corresponds to the determination error. The CNT calculation of J was made by Eq. (11). The smooth curve represents the $\ln J \sim 1/T^2$ approximation of the CNT data. The region studied by ML crystals is highlighted in yellow. **Inset**: Nucleation and activation barriers: W_*/k_BT, Eq. (4), and E_*/k_BT, Eq. (5), *vs.* superheating. Straight lines are approximations of the calculated values.

thermodynamic one, $E_*(T) < W_*(T)$, for all superheatings up to $T = 1.3 \cdot T_L$ (inset in Fig. 5). Such inequality has been previously obtained in similar CNT analyses of LJ and Ge crystallization [99,119,122].

Summarizing, the values of W_*, E_*, n_*, Z_*, and $\mathscr{D}_*$ calculated by the MEAM and two ML models, are shown in Table 2 for all temperatures under investigation. It can be seen that these nucleation parameters in MEAM and ML crystals are consistent. It proves that the constructed ML models are able to correctly reproduce the complex process of crystal decay at the atomic scale.

Inserting Eq. (2) into Eq. (1), one can write.

$$J = \rho \mathscr{D}_* Z_* \exp\left(-3\pi n_*^2 Z_*^2\right) \tag{11}$$

Expression (11) was utilized here to calculate the nucleation rate theoretically, based on physical properties determined from the MD simulations: $\rho, \mathscr{D}_*, Z_*$, and n_*. As a result, the theoretical J falls in the range of $4 \cdot 10^{32} - 2 \cdot 10^{35}$ s^{-1}m^{-3} for the superheatings under investigation, $T/T_L = 1.1 - 1.3$ (Table 1). It should be stressed that these values of J were calculated without any fitting parameter, using only MD-generated data. Fig. 5 summarizes the nucleation rates computed by the MLT and MFPT methods and theoretically calculated by the CNT for the MEAM and ML models. **Excellent agreement of the CNT and MD nucleation rates for both MEAM and ML crystals is found**. The current findings support and reinforce previous computational studies of the spontaneous, homogeneous melting in a simple LJ crystal [42,43,59].

For the ML crystals, the prefactor $\rho \mathscr{D}_* Z_*$ in Eq. (3), determined as the y-axis intercept of the $\ln J(1/T)$ plot, has the same order of magnitude as the theoretical values resulting from the MD simulations, $\rho \mathscr{D}_* Z_* \approx 10^{39}$ s^{-1}m^{-3}. A similar analysis of the MEAM crystals data reveals a huge discrepancy of 10 o.m. in $\rho \mathscr{D}_* Z_*$ values, which is often observed in crystallization studies [99,119]. According to Eq. (3), the slope of the $\ln J(1/T)$ plot determines the height of the nucleation barrier, W_*. In this way, W_* for the MEAM crystals take implausible values of 33–35 $k_B T$, which significantly exceed those calculated from Eq. (4), $W_* = 3\pi n_*^2 Z_*^2 k_B T \approx 11\ k_B T$. In contrast, W_* in the ML models obtained from the $\ln J(1/T)$ plot and from Eq. (4) are identical within the determination error of $1 \cdot k_B T$ (Table 2).

Thus, MD melting in ML crystals is unprecedentedly and accurately described by the CNT not only in the final outcome (the nucleation rate), but also in terms of the underlying details (kinetic prefactor, formation energy and size of critical nucleus).

It should be noted that only spherical critical liquid nuclei were theoretically considered here, even though their formation may not always be energetically favorable even in isotropic crystals [42,123]. However, it has been shown [124] that the formation of lentil-shaped nuclei is only favorable at low superheatings, indicating that the theoretical assumption of spherical nuclei is reasonable for the present estimation at moderate and high superheatings.

In summary, this is the first theoretical and computational study on the spontaneous melting of AlCu crystals described by the MEAM and ML realistic interatomic potentials. Moreover, for the first time, the CNT formalism, utilized with no adjustable parameters, successfully described the melting of a crystal model created through artificial neural network machine learning-processed quantum calculations, that is, the computational model did not rely on hand-crafted interatomic potential functions.

The application of the developed AlCu ML model is not restricted to the scope of this study. It can be utilized to comprehensively explore the complex AlCu phase diagram [125] and investigate potential structural transformations, such as solid–solid transitions via melting [101]. Overall, in the near future, properly designed and trained ML models are expected to essentially enhance our understanding of the fundamental nature of crystal decay at the nanoscale and provide a means to test and develop theoretical models of order–disorder transitions.

Table 2
Nucleation parameters of AlCu liquids for $p = 1$ bar at five superheatings, T/T_L

Quantity	Superheating, T/T_L				
	1.11	1.15	1.20	1.27	1.30
Model	MEAM	MEAM	MEAM	ML-*sl*	ML-*l*
T, K	1300	1350	1400	1050	1150
n_*, MFPT	118	108	84	60	52
R_*, nm	0.78	0.75	0.70	0.61	0.58
Z_*, MFPT	0.010	0.010	0.013	0.017	0.020
ρ, 10^{28} m^{-3}	6.184	6.158	6.129	6.770	6.798
ρ_*, 10^{28} m^{-3}	6.024	5.992	5.961	6.432	6.372
$\mathscr{D}_*$, s^{-1}	$9.9 \cdot 10^{10}$	$2.5 \cdot 10^{11}$	$1.0 \cdot 10^{12}$	$1.3 \cdot 10^{12}$	$3.1 \cdot 10^{12}$
γ, J/m^2	0.084	0.086	0.107	0.093	0.115
$\lvert\Delta g + e\rvert/k_B T$	0.201	0.204	0.268	0.331	0.392
$E_*/k_B T$, Eq. (5)	9.7	8.7	7.1	6.2	5.3
$W_*/k_B T$, Eq. (4)	11.8	11.0	11.2	9.9	10.2
$W_*/k_B T$ from $\ln J(1/T)$	35.2	33.9	32.7	9.9	9.1

4. Conclusion

The present results for spontaneous melting of an AlCu alloy reveal a very good agreement between theoretical nucleation rates calculated by the CNT and values obtained through computer simulations. Furthermore, the CNT correctly described the underlying details of liquid drop nucleation in the ML solid, accurately reproducing the kinetic prefactor and the size, formation energy, and growth velocity of the critical nuclei. Thus, the melting of the AlCu model created through machine learning-processed quantum calculations, that is, not relying on hand-crafted interatomic potential functions, was successfully described by the CNT formalism, without any adjustable parameters.

This research provides a strong validation for the CNT as an effective descriptor of homogeneous nucleation in this superheated material and generalizes the validity of this theory as a powerful tool for analyzing and predicting the kinetics and thermodynamics of first-order phase transitions.

CRediT authorship contribution statement

Azat O. Tipeev: Conceptualization, Methodology, Software, Investigation, Formal analysis, Writing – original draft, Writing – review & editing, Visualization, Supervision, Funding acquisition. **Roman E. Ryltsev:** Software. **Nikolay M. Chtchelkatchev:** Software. **Shiddhartha Ramprakash:** Formal analysis. **Edgar D. Zanotto:** Writing – review & editing, Supervision, Project administration, Funding acquisition.

Declaration of Competing Interest

The authors declare the following financial interests/personal relationships which may be considered as potential competing interests: Azat Tipeev and Edgar Zanotto report financial support was provided by State of Sao Paulo Research Foundation. Roman Ryltsev reports financial support was provided by Ministry of Science and Higher Education of the Russian Federation.

Data availability

The data that support the findings of this study are available from the corresponding author upon reasonable request. The machine learning interatomic potentials for AlCu, developed in this paper, are available in the Zenodo repository via https://doi.org/10.5281/zenodo.7823534.

Acknowledgments

A. Tipeev acknowledges the São Paulo Research Foundation,

FAPESP, Brazil, for the Grant # 2022/05837-5. E. Zanotto would also like to thank FAPESP (contract CEPID # 2013/07793-6) for the financial support to this research. R. Ryltsev was supported by the Ministry of Science and Higher Education of the Russian Federation (state assignment for IMET UB RAS # 122013100200–2). Shiddhartha R. expresses deep gratitude to Ruhr University in Bochum/Germany for the warm hospitality during his DAAD WISE fellowship in 2022. The numerical calculations were performed using the computer facilities of the federal collective usage center 'Complex for Simulation and Data Processing for Mega-science Facilities' at NRC 'Kurchatov Institute' (ckp.nrcki.ru), supercomputers at Joint Supercomputer Center of Russian Academy of Sciences (www.jscc.ru), and 'Uran' supercomputer of IMM UB RAS (parallel.uran.ru). The authors are grateful to José P. Rino from the Federal University of São Carlos, Brazil, and Alexander S. Abyzov from the National Science Center Kharkov Institute of Physics and Technology, Kharkov, Ukraine, for the fruitful discussion and critical comments.

References

[1] G. Tammann, On the behavior of water at high pressure and low temperatures, Z. Phys. Chem. 72 (1910) 609–631.
[2] A.R. Ubbelohde, Melting and crystal structure, Quart. Rev. Chem. Soc. 4 (1950) 356–381.
[3] B. Wunderlich, Macromolecular Physics: Crystal Melting, Academic Press, 1980.
[4] D.R. Uhlmann, On the internal nucleation of melting, J. Non Cryst. Solids 41 (1980) 347–357.
[5] A.O. Tipeev, J.P. Rino, E.D. Zanotto, Direct determination of Lennard-Jones crystal surface free energy by a computational cleavage method, J. Chem. Phys. 155 (2021), 094101.
[6] J.W.P. Schmelzer, A.O. Tipeev, Effect of planar interfaces on nucleation in melting and crystallization, Entropy 24 (2022) 1029.
[7] S.E. Khaikin, N.R. Bene, On the phenomenon of overheating of a solid, C. R. Acad. Sci. URSS 23 (1939) 31.
[8] J. Daeges, H. Gleiter, J.H. Perepezko, Superheating of metal crystals, Phys. Lett. A. 119 (1986) 79–82.
[9] L. Gråbæk, J. Bohr, E. Johnson, A. Johansen, L. Sarholt-Kristensen, H. H. Andersen, Superheating and supercooling of lead precipitates in aluminum, Phys. Rev. Lett. 64 (1990) 934–937.
[10] J. Herman, H. Elsayed-Ali, Superheating of Pb (111), Phys. Rev. Lett. 69 (1992) 1228–1231.
[11] L. Gråbæk, J. Bohr, H.H. Andersen, A. Johansen, E. Johnson, L. Sarholt-Kristensen, I.K. Robinson, Melting, growth, and faceting of lead precipitates in aluminum, Phys. Rev. B 45 (1992) 2628–2637.
[12] L. Zhang, Z.H. Jin, L.H. Zhang, M.L. Sui, K. Lu, Superheating of confined Pb thin films, Phys. Rev. Lett. 85 (2000) 1484–1487.
[13] J. Zhong, L.H. Zhang, Z.H. Jin, M.L. Sui, K. Lu, Superheating of Ag nanoparticles embedded in Ni matrix, Acta Mater. 49 (2001) 2897–2904.
[14] G.I. Kanel, V.E. Fortov, S.V. Razorenov, Shock waves in condensed-state physics, Phys. Usp 50 (2007) 771–791.
[15] V.E. Fortov, L.V. Altshuler, R.F. Trunin, A.I. Funtikov, High-pressure shock compression of solids VII: Shock waves and extreme states of matter, Springer Science & Business Media, 2013.
[16] Y. Zhang, H. Xiong, H.E. Elsayed-Ali, Melting and structural dynamics of indium nanoparticles embedded in aluminum, J. Phys. Chem. C 124 (2020) 19340–19347.
[17] S.-N. Luo, T.J. Ahrens, T. Çağın, A. Strachan, W.A. Goddard III, D.C. Swift, Maximum superheating and undercooling: Systematics, molecular dynamics simulations, and dynamic experiments, Phys. Rev. B 68 (2003), 134206.
[18] J.H. Bilgram, Dynamics at the solid-liquid transition: Experiments at the freezing point, Phys. Rep. 153 (1987) 1–89.
[19] Q.S. Mei, K. Lu, Melting and superheating of crystalline solids: From bulk to nanocrystals, Prog. Mater. Sci. 52 (2007) 1175–1262.
[20] F.A. Lindemann, The calculation of molecular vibration frequencies, Phys. Z. 11 (1910) 609–612.
[21] X. Fan, D. Pan, M. Li, Melting of bcc crystal Ta without the Lindemann criterion, J. Phys. Condens. Matter 31 (2019), 095402.
[22] X. Fan, D. Pan, M. Li, Rethinking Lindemann criterion: A molecular dynamics simulation of surface mediated melting, Acta Mater. 193 (2020) 280–290.
[23] G. Zhang, X. Fan, Q. Zhang, Q. Li, Y. Wu, M. Li, Partial disordering and homogeneous melting in multicomponent systems, Acta Mater. 239 (2022), 118281.
[24] M. Born, Thermodynamics of crystals and melting, J. Chem. Phys. 7 (1939) 591–603.
[25] K. Lu, Y. Li, Homogeneous nucleation catastrophe as a kinetic stability limit for superheated crystal, Phys. Rev. Lett. 80 (1998) 4474–4477.
[26] B. Rethfeld, K. Sokolowski-Tinten, D. von der Linde, S.I. Anisimov, Ultrafast thermal melting of laser-excited solids by homogeneous nucleation, Phys. Rev. B 65 (2002), 092103.
[27] G.S. Smirnov, V.V. Stegailov, Melting and superheating of sI methane hydrate: Molecular dynamics study, J. Chem. Phys. 136 (2012), 044523.
[28] V.P. Skripov, Metastable liquids, Nauka, Moscow, 1972, Wiley, New York, 1974.
[29] G.T. Avedisian, The homogeneous nucleation limits of liquids, J. Phys. Chem. Ref. Data 14 (1985) 695–729.
[30] V.P. Skripov, V.P. Koverda, Spontaneous crystallization of supercooled liquids, Nauka, Moscow, 1984.
[31] K.F. Kelton, A.L. Greer, Nucleation in condensed matter: applications in materials and biology, 1st Ed., Pergamon, U.K., 2010.
[32] A.L. Roitburd, Modified Clausius-Clapeyron equation for the hysteresis of phase transformations in solids, Sov. Phys. Solid State 25 (1983) 33–40.
[33] Y.B. Zeldovich, Contribution to the theory of the formation of a new phase, J. Exp. Theor. Phys. 12 (1942) 525–538.
[34] D. Turnbull, J.C. Fisher, Rate of nucleation in condensed systems, J. Chem. Phys. 17 (1949) 71–73.
[35] V.P. Skripov, V.P. Koverda, V.N. Skokov, Size effect on melting of small particles, Phys. Stat. Sol. (a) 66 (1981) 109–118.
[36] Z. Wang, F. Wang, Y. Peng, Z. Zheng, Y. Han, Imaging the homogeneous nucleation during the melting of superheated colloidal crystals, Science 338 (2012) 87–90.
[37] Z. Wang, F. Wang, Y. Peng, Y. Han, Direct observation of liquid nucleus growth in homogeneous melting of colloidal crystals, Nat. Commun. 6 (2015) 7942.
[38] H. Hwang, D.A. Weitz, F. Spaepen, Direct observation of crystallization and melting with colloids, Proc. Natl. Acad. Sci. 116 (2019) 1180–1184.
[39] M.A. Sharaf, R.A. Dobbins, A comparison of measured nucleation rates with the predictions of several theories of homogeneous nucleation, J. Chem. Phys. 77 (1982) 1517–1526.
[40] G.C. Sosso, J. Chen, S.J. Cox, M. Fitzner, P. Pedevilla, A. Zen, A. Michaelides, Crystal nucleation in liquids: Open questions and future challenges in molecular dynamics simulations, Chem. Rev. 116 (2016) 7078–7116.
[41] Z.H. Jin, P. Gumbsch, K. Lu, E. Ma, Melting mechanisms at the limit of superheating, Phys. Rev. Lett. 87 (2001), 055703.
[42] V.G. Baidakov, A.O. Tipeev, Nucleation of liquid droplets and voids in a stretched Lennard-Jones fcc crystal, J. Chem. Phys. 143 (2015), 124501.
[43] V.G. Baidakov, A.O. Tipeev, Mechanical instability and nucleation in a Lennard-Jones fcc crystal at limiting stretching, Chem. Phys. Lett. 643 (2016) 6–9.
[44] M. Forsblom, G. Grimvall, How superheated crystals melt, Nat. Mater. 4 (2005) 388–390.
[45] A.Y. Kuksin, G.E. Norman, V.V. Stegailov, A.V. Yanilkin, Model of Al crystal fracture under high-rate strain based on molecular-dynamic simulations, Physico-Chemical Kinetics in Gas, Dynamics 7 (2008) 1–6.
[46] A. Kuksin, G. Norman, V. Stegailov, A. Yanilkin, P. Zhilyaev, Dynamic fracture kinetics, influence of temperature and microstructure in the atomistic model of aluminum, Int. J. Fract. 162 (2010) 127–136.
[47] C. Rincent, J.-R. Castillo-Sánchez, A.E. Gheribi, J.-P. Harvey, On the exploration of the melting behavior of metallic compounds and solid solutions via multiple classical molecular dynamics approaches: application to Al-based systems, Phys. Chem. Chem. Phys. 25 (2023) 10866–10884.
[48] V. Stegailov, Homogeneous and heterogeneous mechanisms of superheated solid melting and decay, Comput. Phys. Commun. 169 (2005) 247–250.
[49] X. Fan, X. Chen, D. Pan, Y. Liu, P. Liu, M. Li, Localization and delocationzation of surface disordering in surface mediated melting, Phys. Rev. B 104 (2021), 134204.
[50] T.P. Duy, V.V. Hoang, Atomic mechanism of homogeneous melting of bcc Fe at the limit of superheating, Physica B Condens. Matter 407 (2012) 978–984.
[51] R. Sun, Z. Feng, S. Gao, P. Liu, H. Qi, N. Song, Using molecular dynamic simulations to describe the solid-liquid phase transition of lead nanoparticles with different nano-geometries, IOP SciNotes 1 (2020), 024807.
[52] S. Liang, L. Yi, D. Liang, Molecular insights into the homogeneous melting of methane hydrates, J. Phys. Chem. C 118 (2014) 28542–28547.
[53] K. Mochizuki, Computational study on homogeneous melting of benzene phase I, Crystals 9 (2019) 84.
[54] D. Donadio, P. Raiteri, M. Parrinello, Topological defects and bulk melting of hexagonal ice, J. Phys. Chem. B 109 (2005) 5421–5424.
[55] K. Mochizuki, M. Matsumoto, I. Ohmine, Defect pair separation as the controlling step in homogeneous ice melting, Nature 498 (2013) 350–354.
[56] C. Moritz, P.L. Geissler, C. Dellago, The microscopic mechanism of bulk melting of ice, J. Chem. Phys. 155 (2021), 124501.
[57] G.E. Norman, V.V. Stegailov, Homogeneous nucleation in a superheated crystal. Molecular-dynamic simulation, Dokl. Akad. Nauk 386 (2002) 328–332.
[58] G.E. Norman, V.V. Stegailov, Simulation of ideal crystal superheating and decay, Mol. Simul. 30 (2004) 397–406.
[59] V.G. Baidakov, A.O. Tipeev, Molecular dynamics simulation of homogeneous nucleation in a superheated Lennard-Jones crystal, J. Non. Cryst. Sol. 503 (2019) 302–307.
[60] E.A. Starke Jr, J.T. Staley, Application of modern aluminum alloys to aircraft, Prog. Aerosp. Sci. 32 (1996) 131–172.
[61] Z. Huda, N.I. Taib, T. Zaharinie, Characterization of 2024–T3: An aerospace aluminum alloy, Mater. Chem. Phys. 113 (2009) 515–517.
[62] P. Rambabu, N. Eswara Prasad, V.V. Kutumbarao, R.J.H. Wanhill, Aluminium Alloys for Aerospace Applications, In: Aerospace Materials and Material Technologies, Indian Institute of Metals Series, Springer, Singapore, 2017.
[63] S.A. Kuryntsev, Review: laser welding of dissimilar materials (Al/Fe, Al/Ti, Al/Cu) – methods and techniques, microstructure and properties, Materials 15 (2022) 122.
[64] S. Terzi, L. Salvo, M. Suéry, E. Boller, In situ X-ray microtomography characterization of the entrapped liquid formed during partial remelting of a cold-rolled Al–8 wt.% Cu alloy, Scr. Mater. 60 (2009) 671–674.

[65] S. Fischer, M. Rettenmayr, Observation of early melting stages of an Al–Cu alloy in a temperature gradient, Int. J. Mater. Res. 102 (2011) 1226–1231.
[66] S. Terzi, L. Salvo, M. Suéry, A.K. Dahle, E. Boller, Internal melting and coarsening of liquid droplets in an Al–Cu alloy: a 4-D experimental study, J. Mater. Sci. 48 (2013) 7422–7434.
[67] S. Lippmann, M. Fink, M. Rettenmayr, Experimental determination of the nucleation rate of melt in a solid solution, Acta Mater. 72 (2014) 32–40.
[68] S. Lippmann, C. Simon, S. Zechel, M. Seyring, U.S. Schubert, G. Wilde, M. Rettenmayr, Determining solid/liquid interfacial energies in Al-Cu by curvature controlled melting point depression, Acta Mater. 147 (2018) 113–121.
[69] D.W. Oxtoby, D. Kashchiev, A general relation between the nucleation work and the size of the nucleus in multicomponent nucleation, J. Chem. Phys. 100 (1994) 7665–7671.
[70] J.W.P. Schmelzer, On the determination of the kinetic pre-factor in classical nucleation theory, J. Non. Cryst. Sol. 356 (2010) 2901–2907.
[71] J.R. Castillo-Sánchez, A. Rincent, A.E. Gheribi, J.P. Harvey, On the transferability of classical pairwise additive atomistic force field to the description of unary and multi-component systems: applications to the solidification of Al-based alloys, Phys. Chem. Chem. Phys. 24 (2022) 22605–22623.
[72] D.R. Cassar, A.C.P.L.F. de Carvalho, E.D. Zanotto, Predicting glass transition temperatures using neural networks, Acta Mater. 159 (2018) 249–256.
[73] H. Liu, Z. Fu, K. Yang, X. Xu, M. Bauchy, Machine learning for glass science and engineering: A review, J. Non. Cryst. Sol. X 4 (2019), 100036.
[74] E. Alcobaça, S.M. Mastelini, T. Botari, B.A. Pimentel, D.R. Cassar, A.C.P.L.F. de Carvalho, E.D. Zanotto, Explainable machine learning algorithms for predicting glass transition temperatures, Acta Mater. 188 (2020) 92–100.
[75] Z. Wei, J. Yu, Y. Lu, J. Han, C. Wang, X. Liu, Prediction of diffusion coefficients in fcc, bcc and hcp phases remained stable or metastable by the machine-learning methods, Mater. Des. 198 (2021), 109287.
[76] S.M. Mastelini, D.R. Cassar, E. Alcobaça, T. Botari, A.C.P.L.F. de Carvalho, E. D. Zanotto, Machine learning unveils composition-property relationships in chalcogenide glasses, Acta Mater. 240 (2022), 118302.
[77] Q.-J. Honga, S.V. Ushakov, A. van de Walle, A. Navrotsky, Melting temperature prediction using a graph neural network model: From ancient minerals to new materials, Proc. Natl. Acad. Sci. 119 (2022).
[78] F. Oviedo, J.L. Ferres, T. Buonassisi, K.T. Butler, Interpretable and explainable machine learning for materials science and chemistry, Acc. Mater. Res. 3 (2022) 597–607.
[79] S. Axelrod, D. Schwalbe-Koda, S. Mohapatra, J. Damewood, K.P. Greenman, R. Gómez-Bombarelli, Learning matter: materials design with machine learning and atomistic simulations, Acc. Mater. Res. 3 (2022) 343–357.
[80] V.L. Deringer, M.A. Caro, G. Csányi, Machine learning interatomic potentials as emerging tools for materials science, Adv. Mater. 31 (2019) 1902765.
[81] Y. Mishin, Machine-learning interatomic potentials for materials science, Acta Mater. 214 (2021), 116980.
[82] J. Behler, G. Csányi, Machine learning potentials for extended systems: a perspective, Eur. Phys. J. B 94 (2021) 142.
[83] T. Wen, L. Zhang, H. Wang, E. Weinan, D.J. Srolovitz, Deep potentials for materials science, Mater. Futures 1 (2022), 022601.
[84] J.D. Morrow, J.L.A. Gardner, V.L. Deringer, How to validate machine-learned interatomic potentials, J. Chem. Phys. 158 (2023), 121501.
[85] H. Niu, L. Bonati, P.M. Piaggi, M. Parrinello, Ab initio phase diagram and nucleation of gallium, Nat. Commun. 11 (2020) 2654.
[86] A. Mahata, T. Mukhopadhyay, M.A. Zaeem, Modified embedded-atom method interatomic potentials for Al-Cu, Al-Fe and Al-Ni binary alloys: From room temperature to melting point, Comput. Mater. Sci. 201 (2022), 110902.
[87] M.I. Baskes, Modified embedded-atom potentials for cubic materials and impurities, Phys. Rev. B 46 (1992) 2727–2742.
[88] M.I. Baskes, R.A. Johnson, Modified embedded atom potentials for HCP metals, Modell. Simul. Mater. Sci. Eng. 2 (1994) 147–163.
[89] B.-J. Lee, M.I. Baskes, Second nearest-neighbor modified embedded-atom-method potential, Phys. Rev. B 62 (2000) 8564.
[90] B.-J. Lee, M.I. Baskes, H. Kim, Y.K. Cho, Second nearest-neighbor modified embedded atom method potentials for bcc transition metals, Phys. Rev. B 64 (2001), 184102.
[91] I.A. Balyakin, R.E. Ryltsev, N.M. Chtchelkatchev, Liquid-solid structural inheritance in machine-learning interatomic potentials for network-forming systems, JETP Lett. 117 (2023) 370–376.
[92] G. Kresse, J. Furthmuller, Efficiency of ab-initio total energy calculations for metals and semiconductors using a plane-wave basis set, Comput. Mater. Sci. 6 (1996) 15–50.
[93] R.E. Ryltsev, N.M. Chtchelkatchev, Deep machine learning potentials for multicomponent metallic melts: Development, predictability and compositional transferability, J. Mol. Liq. 349 (2022), 118181.
[94] E.O. Hazieva, N.M. Chtchelkatchev, A.O. Tipeev, R.E. Ryltsev, Accuracy, performance and transferability of interparticle potentials for Al-Cu alloys: comparison of embedded atom and deep machine learning models, J. Exp. Theor. Phys. (2023) (Accepted).
[95] G. Pilania, J.E. Gubernatis, T. Lookman, Structure classification and melting temperature prediction in octet AB solids via machine learning, Phys. Rev. B 91 (2015), 214302.
[96] R. Jinnouchi, F. Karsai, G. Kresse, On-the-fly machine learning force field generation: Application to melting points, Phys. Rev. B 100 (2019), 014105.
[97] D. Marchand, A. Jain, A. Glensk, W.A. Curtin, Machine learning for metallurgy I. A neural-network potential for Al-Cu, Phys. Rev. Mater. 4 (2020), 103601.
[98] J.R. Morris, C.Z. Wang, K.M. Ho, C.T. Chan, Melting line of aluminum from simulations of coexisting phases, Phys. Rev. B 49 (1994) 3109–3115.
[99] A.O. Tipeev, E.D. Zanotto, J.P. Rino, Crystal nucleation kinetics in supercooled germanium: MD simulations versus experimental data, J. Phys. Chem. B 124 (2020) 7979–7988.
[100] O. Zobac, A. Kroupa, A. Zemanova, K.W. Richter, Experimental description of the Al-Cu binary phase diagram, Metall. Mater. Trans. A 50 (2019) 3805–3815.
[101] S. Pogatscher, D. Leutenegger, J.E. Schawe, P.J. Uggowitzer, J.F. Löffler, Solid–solid phase transitions via melting in metals, Nat. Commun. 7 (2016) 11113.
[102] S. Plimpton, Fast parallel algorithms for short-range molecular dynamics, J. Comput. Phys. 117 (1995) 1–19.
[103] A.P. Thompson, H.M. Aktulga, R. Berger, D.S. Bolintineanu, W.M. Brown, P. S. Crozier, P.J. in 't Veld, A. Kohlmeyer, S.G. Moore, T.D. Nguyen, R. Shan, M. J. Stevens, J. Tranchida, C. Trott, S.J. Plimpton, LAMMPS-a flexible simulation tool for particle-based materials modeling at the atomic, meso, and continuum scales, Comput. Phys. Commun. 271 (2022), 108171.
[104] A.T. Bharucha-Reid, Elements of the theory of Markov processes and their application, McGraw Hill, New York, 1960.
[105] V.G. Baidakov, A.O. Tipeev, On two approaches to determination of the nucleation rate of a new phase in computer experiments, Thermochim. Acta 522 (2011) 14–19.
[106] T. Kinjo, M. Matsumoto, Cavitation processes and negative pressure, Fluid Phase Equilib. 144 (1998) 343–350.
[107] V.G. Baidakov, S.P. Protsenko, Computer simulation of nucleation in a liquid under tension, Dokl. Phys. 49 (2004) 69–72.
[108] V.G. Baidakov, A.O. Tipeev, K.S. Bobrov, G.V. Ionov, Crystal nucleation rate isotherms in Lennard-Jones liquids, J. Chem. Phys. 132 (2010), 234505.
[109] C.W. Gardiner, Handbook of stochastic methods for physics chemistry and the natural sciences, 2nd ed., Springer, 1997.
[110] J. Wedekind, R. Strey, D. Requera, New method to analyze simulations of activated processes, J. Chem. Phys. 126 (2007), 134103.
[111] J. Wedekind, D. Requera, Kinetic reconstruction of the free-energy landscape, J. Phys. Chem. B 112 (2008) 11060–11063.
[112] K. Song, D.E. Makarov, E. Vouga, The effect of time resolution on the observed first passage times in diffusive dynamics, J. Chem. Phys. 158 (2023), 111101.
[113] J. Wedekind, G. Chkonia, J. Wölk, R. Strey, D. Reguera, Crossover from nucleation to spinodal decomposition in a condensing vapor, J. Chem. Phys. 131 (2009), 114506.
[114] S.E.M. Lundrigan, I. Saika-Voivod, Test of classical nucleation theory and mean first-passage time formalism on crystallization in the Lennard-Jones liquid, J. Chem. Phys. 131 (2009), 104503.
[115] V.G. Baidakov, A.O. Tipeev, Crystal nucleation and the solid–liquid interfacial free energy, J. Chem. Phys. 136 (2012), 074510.
[116] A.R. Kurochkin, P.S. Popel, D.A. Yagodin, A.V. Borisenko, A.V. Okhapkin, Density of Copper-Aluminum alloys at temperatures up to 1400°C determined by the gamma-ray technique, High Temp. 51 (2013) 197–205.
[117] V.G. Baidakov, Spontaneous cavitation in a Lennard-Jones liquid: Molecular dynamics simulation and the van der Waals-Cahn-Hilliard gradient theory, J. Chem. Phys. 144 (2016), 074502.
[118] B.J. Block, S.K. Das, M. Oettel, P. Virnau, K. Binder, Curvature dependence of surface free energy of liquid drops and bubbles: A simulation study, J. Chem. Phys. 133 (2010), 154702.
[119] A.O. Tipeev, E.D. Zanotto, J.P. Rino, Diffusivity, interfacial free energy, and crystal nucleation in a supercooled Lennard-Jones liquid, J. Phys. Chem. C 122 (2018) 28884–28894.
[120] M. Gündüz, J.D. Hunt, The measurement of solid-liquid surface energies in the Al-Cu, Al-Si and Pb-Sn systems, Acta Metall. Mater. 33 (1985) 1651–1672.
[121] G.A. Somorjai, Y. Li, Introduction to surface chemistry and catalysis, 2nd ed., Wiley, 2010.
[122] A.O. Tipeev, J.P. Rino, E.D. Zanotto, Unveiling relaxation and crystal nucleation interplay in supercooled germanium liquid, Acta Mater. 220 (2021), 117303.
[123] V.I. Motorin, S.L. Musher, Kinetics of the volume melting. Nucleation and superheating of metals, J. Chem. Phys. 81 (1984) 465–469.
[124] E.A. Brener, S.V. Iordanskii, V.I. Marchenko, Elastic effects on the kinetics of a phase transition, Phys. Rev. Lett. 82 (1999) 1506–1509.
[125] N. Ponweiser, C.L. Lengauer, K.W. Richter, Re-investigation of phase equilibria in the system Al–Cu and structural analysis of the high-temperature phase η_1-$Al_{1-\delta}Cu$, Intermetallics 19 (2011) 1737–1746.